Short Title:

Regulation of photosynthetic control

Title:

The algal PETC-Pro171-Leu suppresses electron transfer in the cytochrome b_6f under acidic lumenal condition

Authors:

Shin-Ichiro Ozawa[a], Felix Buchert[b], Ruby Reuys[b], Michael Hippler[a, b], and Yuichiro Takahashi[c]

Author affiliations:

[a]Institute of Plant Science and Resources, Okayama University, Kurashiki, 710-0046, Japan

[b]Institute of Plant Biology and Biotechnology, University of Münster, 48143 Münster, Germany

[c]Research Institute for Interdisciplinary Science, Okayama University, Okayama, 700-8530, Japan

One sentence summary:

Change of PETC to P171L via site directed mutagenesis alters the pH dependency of the photosynthetic control mechanism

Author Contributions:

S.O., F.B., M.H., and Y.T. conceived the original screening and research plans; S.O., F.B., M.H., and Y.T. supervised the experiments; S.O., F.B., and R.R. designed and performed the experiments; S.O., F.B., and R.R. analyzed the data; S.O., F.B., M.H., and Y.T. conceived the project and wrote the article with contributions of all the authors; S.O., F.B., M.H., and Y.T. supervised and completed the writing. S.O. agrees to serve as the author responsible for contact and ensures communication.

Funding:

This work was supported by the Grants-in-Aid for Scientific Research from Japan Society for the Promotion of Science KAKENHI JP21K06217 (to S.O.) and the JP16H06554 and 21H02510 (to Y.T.). M.H. acknowledges funding from the Deutsche Forschungsgemeinschaft (739/13-2) and by the RECTOR program (Okayama University, Japan).

Responsibilities of the Author for Contact:

Shin-Ichiro Ozawa

Institute of Plant Science and Resources, Okayama University, Okayama 710-0046, Japan

1 Phone: +81-86-434-1225, E-mail: OzwSh1r@okayama-u.ac.jp

2 **Keywords:**

3 photosynthesis, Q-cycle, cytochrome b_6f, photosynthetic control

Abstract

Linear photosynthetic electron flow (LEF) produces NADPH and generates a proton electrochemical potential gradient across the thylakoid membrane used to synthesize ATP, both of which are required for CO_2 fixation. As cellular demand for ATP and NADPH are variable, cyclic electron flow (CEF) between PSI and cytochrome b_6f complex (b_6f) produces extra ATP. The b_6f regulates LEF and CEF via photosynthetic control, which is a pH-dependent b_6f slowdown of plastoquinol oxidation at the lumenal site. This protection mechanism is triggered at more alkaline lumen pH in the *pgr1* mutant of the vascular plant *Arabidopsis thaliana*, carrying Pro194Leu in the b_6f Rieske Iron-sulfur protein. In this work, we introduced *pgr1* mutation in the green alga *Chlamydomonas reinhardtii* (*PETC-P171L*). Consistent with *pgr1* phenotype, *PETC-P171L* displayed a limited photosynthesis along with slower photoautotrophic growth under high light conditions. Our data under low oxygen revealed that the ΔpH component in algae was already sufficient to trigger the effect in *PETC-P171L* in sub-saturating light conditions where the mutant b_6f was more restricted to oxidize the PQ pool and revealed a diminished electron flow.

Introduction

Oxygenic photosynthesis fixes carbon dioxide and generates oxygen as a result of intra- and intermolecular photochemical electron transfer reactions. The electron transfer pathways in oxygenic photosynthesis either follows Linear Electron Flow (LEF) or, as an example of alternative passages, Cyclic Electron Flow (CEF). Electrons stemming from water oxidation reduce $NADP^+$ during LEF, thus providing the reducing power for CO_2 fixation in the Calvin Benson cycle. In the CEF, electrons from reduced ferredoxin (Fd) are differently partitioned and redirected into the plastoquinone (PQ) pool. A possible CEF route reinjects electrons into the cytochrome b_6f complex (b_6f) from the stromal side. In LEF and CEF, the b_6f contributes to proton gradient formation across thylakoid membrane by translocating protons from chloroplast stroma to thylakoid lumen. Light-driven charge separation, water splitting as well as b_6f activity generate a membrane potential ($\Delta\Psi$) and a proton gradient (ΔpH), respectively, and this proton motive force (*pmf*) drives ATP synthesis. During prolonged electron transfer, the lumen will get further acidified, which in turn will slow down plastoquinol (PQH_2) oxidation at the Qo-site of b_6f, and thereby establish photosynthetic control to protect photosystem I (PSI) from acceptor side limitation (Rumberg and Siggel, 1969; Tikhonov et al., 1981; Nishio and Whitmarsh, 1993). Lumen acidification is also important to induce Non-Photochemical Quenching (NPQ) (Kanazawa and Kramer, 2002), which is the most rapid photoprotective response to excess light. The fastest constituent of NPQ is qE, which operates at a time scale of seconds to minutes and regulates the thermal dissipation of excess absorbed light energy, thereby providing effective photo-protection of photosystem II (PSII). In vascular plants, the PSII protein PSBS is essential for qE (Li et al, 2000), whereas qE induction in the green alga *Chlamydomonas reinhardtii* is mediated by LHCSR3, an ancient light-harvesting protein that is missing in vascular plants (Peers et al., 2009).

Electron transfer through the b_6f is governed by the light-induced introduction of an electron hole (positive charge) into the high-potential chain. The latter involves redox centers heme *f* and the [2Fe-2S] type Rieske Iron Sulfur Cluster (Rieske ISC). The electron hole depends on photo-oxidized plastocyanin and is successively passed from heme *f* via Rieske ISC to PQH_2. The Q-cycle within the b_6f is responsible to generate a *pmf* across the thylakoid membrane, owing to a sophisticated electron bifurcation. Two electrons are pulled from PQH_2 at the Q_o site, forming PQ within the membrane

while simultaneously releasing two H^+ into the lumen. During the PQH_2 oxidation at the Q_o site, the first electron is transferred into the high-potential chain (Rieske ISC reducing heme *f*), and the second electron into the low-potential chain (b_L heme reducing b_H heme, terminal acceptor is c_i heme). A second PQH_2 oxidation at the Q_o site forms a reduced form of b_H / c_i heme pair which reduces a PQ bound at Q_i site to complete the Q-cycle (note that alternative annotations for Q_o, Q_i, b_H and c_i can be found in literatures). It was suggested that under LEF and CEF conditions two types of Q-cycle mechanism operate in the b_6f with specific lumen acidification efficiencies per electron transferred via the high-potential chain (Buchert et al., 2020).

The molecular structure of b_6f complex was first resolved in the green alga *Chlamydomonas reinhardtii* and the cyanobacteria *Mastigocladus laminosus* independently (Kurisu et al., 2003; Stroebel et al., 2003). The b_6f functions as a homodimer, and each monomer consists of four core subunits (PetA, PetB, PETC, and PetD) and four stably associated small subunits (PetG, PetL, PETM, and PETN) to stabilize the complex (Figure 1A). The cofactors and quinone binding pockets involved in electron transfer are found in the b_6f core subunits which resemble the cytochrome bc_1 complex of the respiratory chain. The structure-function similarities suggest that the hydrophilic domain of PETC subunit would move toward PetA subunit in transferring the electrons from Rieske ISC to heme *f*.

In *Arabidopsis thaliana*, various photosynthetic mutants have been isolated and characterized by forward genetics. One study employed ethyl methanesulfonate as mutagen to isolate the CE10-10-1 mutant which exhibited reduced NPQ with normal PSI/PSII quantum yields (Shikanai et al., 1999). A follow-up study pinpointed the mutation as a proline-to-leucine substitution at position 194 of Arabidopsis PETC, linking the NPQ defect to insufficient ΔpH formation in the light (Munekage et al., 2001). The Arabidopsis PETC-P194L mutation was dubbed *pgr1* (*proton gradient regulation* 1).

It is known that green algal photosystems are protected from excess light illumination differently than plants. For instance, algal state transition redistributes excitation energy more effectively than plant (Delepelaire and Wollman, 1985). Moreover, flavodiiron protein was found in algae to protect PSI acceptor side limitation induced by fluctuating light illumination (Jokel et al., 2018). Induction of qE relies on LHCSR3, which requires a preceding stress period to trigger light to heat dissipation upon lumen acidification (Peers et al., 2009; Bonente et al., 2011). Moreover, the algal PETO protein

interacts with b_6f and functions as a CEF effector~~s~~ under anoxic condition, which might point to a different CEF regulation (Takahashi et al., 2016; Buchert et al., 2018).

Herein, we introduced the Arabidopsis *pgr1* mutation into *Chlamydomonas reinhardtii* (*PETC-P171L*) to analyze the effects of the mutation on Photosynthetic Control in the green alga. The *PETC-P171L* cytochrome b_6f showed a normal accumulation and electron flow activity in cells grown under oxic conditions. However, unlike Arabidopsis *pgr1* mutant, the *PETC-P171L* displayed an impaired photoautotrophic growth because the electron transfer activity of the mutated b_6f was significantly decreased in cells grown under anoxic conditions. Our experiments also revealed that the ΔpH component in *PETC-P171L* is dependent on oxygen availability under light conditions that are permissive under other circumstances. Under low oxygen condition the mutant b_6f was more restricted to oxidize the PQ pool and limited electron flow.

Materials and methods

Strains and growth condition

The cells of *Chlamydomonas reinhardtii* were grown in Tris-acetate phosphate (TAP), Tris-Phosphate (TP) medium, or minimum medium (MM) (Harris, 1988) under 50-100 μmol photons·m^{-2}·s^{-1} or 600 μmol photons·m^{-2}·s^{-1}. The previously isolated PETC gene disrupted strain *petC-Δ1* (mating type minus) described in (de Vitry et al., 1999) was crossed with cc-125 (mating type plus) and the resultant PETC deficient progeny was used as a recipient strain for transformation. Doubling time of the cell growth is calculated by dividing 0.30 by specific growth rate obtained as the slope which is computed by linear approximation for logarithmic growth curve in common logarithmic axis. Linear fitting was performed at the highest coefficient of determination (R-square) with no restrictions by using built-in linear fitting program of the Origin Pro 2021b version 9.8.5.212 (OriginLab corporation, USA). Refer the Appendix 1 for derivation of the formula to calculate the doubling time with specific growth rate.

Generation of transformation vectors

The BamHI fragment containing PETC gene (Cre11.g467689.t1.1, Chlamydomonas version 5.5) in the pACR4.5 (de Vitry et al., 1999) was digested with BamHI and subsequently the resulting 4153 bp fragment containing the *PETC* gene and 528 bp upstream of 5' -UTR of PETC was recloned into pBSSK$^-$ vector at BamHI site to yield pgcC plasmid. The mutation Pro171Leu in PETC was introduced by In-Fusion^R (Clontech, TAKARA, Japan) with the DNA fragment between BbvCI and SnaBI sites which was generated by PCR with If-BbvCI_P171L_gcC_F and If-SnaBI_gcC_R primers. The sequence of this study's oligos is shown in Table 1. The DNA sequence of the inserted PCR product was validated by DNA sequencing with the primers used to generate the PCR product and we obtained pgcC-P171L plasmid.

We also prepared the DNA construct in which the *PETC* gene expression is controlled by Chlamydomonas *PSAD* promoter and UTRs. We amplified spliced *PETC* coding DNA sequence fragment by nested PCR with cDNA library as a template DNA. The 1st round of PCR from cDNA library with primers HK#1483 and HK#1484 generated a 731 bp DNA fragment. The following 2nd

round of PCR from the 1000 times diluted 1st round of PCR product with primers HK#1485 and HK#1486. The resulting DNA fragment of the PCR was ligated into the pSL18 vector (Depège et al., 2003) digested with NdeI and XbaI. The cloned DNA sequence of spliced *PETC* coding DNA sequence was validated by DNA sequencing with HK#1491 and HK#1492 primers. To introduce Pro171Leu in PETC, the *PETC* coding DNA sequence was replaced by In-Fusion HD cloning kit at NdeI and XbaI site with the PCR product consisting of two overlapping DNA fragments generated by the following primers; one fragment is generated with If-paDcC-NdeI_F and ccC_mP171L_R while the other fragment is generated with ccC_mP171L_F and If-paDcC-XbaI_R. The replaced DNA sequence was validated by DNA sequencing with the primers used to generate PCR product and cC_cdn131-137_F and cC_cdn137-131_R, and we obtained pccC-P171L plasmid.

Nuclear gene transformation

Nuclear transformation was performed with NEPA21 (Nepagene, Japan) according to the previous research (Yamano et al., 2013). The plasmid DNA was linearized by digesting with ScaI and the digested DNA was delivered into the Δ*PETC*. Selection of transformants was performed on MM solid medium under continuous illumination (50-100 μmol photons·m^{-2}·s^{-1}).

SDS-PAGE

The whole cellular proteins were denatured by heating at 100°C for 2 minutes in the presence of SDS and DTT and the polypeptides were separated by SDS-PAGE (Figures 2, 3, 7 and 8). Subsequent solubilization of dried pellets and SDS-PAGE conditions were as above. The polypeptides were transferred on nitrocellulose membrane for immunodetection. The signals were visualized with a CCD camera equipped imagers (Amersham Imager, LAS-4000, GE healthcare, or Chemidoc, Biorad) and the signal intensities were quantified with Multigauge ver. 3.0 (FujiFilm, Japan)

Low temperature fluorescence emission spectra

Cells were resuspended in TP medium at 2 μg Chl·mL^{-1} and incubated for overnight under illumination at 300 μmol photons·m^{-2}·s^{-1} prior to measurements. After the incubation, culture was

directly, state 1 inducible treatment, or state 2 inducible treatment at 25°C. For the case of state 1 inducible treatment, cells were incubated under 300 µmol photons·m^{-2}·s^{-1} in the presence of 10 µM of 3-(3,4-dichlorophenyl)-1,1-dimethylurea (DCMU). For the case of state 2 inducible treatment, cells were incubated in the darkness in the presence of 100 mM glucose and 50 U·mL^{-1} of glucose oxidase. A sample in a NMR tube was in liquid nitrogen, excited with 430 nm illumination, and emission spectrum was recorded from 400 to 800 nm with FL-7000 (Hitachi, Japan).

***In vivo* Spectroscopy**

For *in vivo* spectrophotometric analysis, cells were maintained at 20 µmol photons·m^{-2}·s^{-1} on agar-supplemented TAP plates (Sueoka, 1960). When growing cells for experiments, liquid TP medium was used. The cultures were grown at 40 µmol photons·m^{-2}·s^{-1} (16 h light/8 h dark) and were bubbled with sterile air at 25°C while shaking at 120 rpm. Cells were harvested after ~2-h in the light cycle. Grown cultures were diluted ~6-fold at least once after inoculation and grown to a density of ~1 ×10^6 cells·mL^{-1} before harvesting (5000 rpm, 5 min, 25°C). Cells were resuspended at 20 µg Chlorophyll·mL^{-1} in TP supplemented with 20% (*w*/*v*) Ficoll. Oxic samples were resuspended throughout the measurements in 2 mL open cuvettes. For oxygen-deprived conditions, cells were supplemented with 50 mM glucose, 10 U glucose oxidase (Carl Roth, Germany) and 30 U catalase (Sigma-Aldrich, USA) in the cuvette, and then overlaid with mineral oil for 20 min in the dark. The enzyme stock solutions to obtain anoxic samples were freshly prepared. Cell incubation in the presence of 10 µM nigericin (from 10 mM ethanolic stock) was carried out for 20 min in the light before the measurements. All samples were light-adapted in the cuvette for 20 min before the measurements using LEDs emitting ~150 µmol photons·m^{-2}·s^{-1} of 630 nm actinic light (AL). Measurements of the electrochromic shift (ECS) and P700 were obtained using a Joliot-type spectrophotometer (JTS-10, Biologic France in Figure 4; JTS-150, Spectrologix USA in Figure 5) and are described in detail elsewhere (Buchert et al., 2020). In brief, all absorption changes were normalized to the ECS ΔI/I signals (520 nm – 546 nm) produced after a saturating 6-ns laser flash in the presence of 1 mM hydroxylamine (HA) and 10 µM DCMU, which relate to the density of active PSI centers in the sample. Thus, the unit of 1 charge separation·PSI^{-1} is produced when measuring the

flash-induced ECS amplitude (rapidly established before the first detection at ~300-ms). This optical ruler was determined in separate measurements to compare sample activities regardless of the presence of HA and DCMU. The shown flash-induced ECS kinetics were obtained after lowering the flash intensity to 30-45% saturation to avoid double turnovers of the cytochrome b_6f complex. The ECS was also deconvoluted in the dark pulse method (Joliot and Joliot, 2002; reviewed in Bailleul et al., 2010; Nawrocki et al., 2019). Accordingly, AL-adapted cells experienced 30 s darkness and were re-illuminated with AL (Supplemental Figure 1). During this 10 s AL induction phase, activities of stable charge separations$\cdot s^{-1} \cdot PSI^{-1}$ were measured by brief light shuttering at discrete time points (four technical replicates with 1 min AL in between; data assembly from two independent measurement sequences). For AL interruptions at t = 0 ms, the linear ECS slopes before (S_L from –4 ms to –1 ms) and after darkness (S_D from +1 ms to +5 ms) gave electron transfer rates before darkness ($S_L - S_D$). Rates at 1 ms illumination of light-adapted cells were calculated from separate slopes obtained during 2 ms AL after 30 s dark (15 replicates spaced by 5 s). P700 measurements (705 nm – 740 nm) are based on the method by (Klughammer and Schreiber, 1994), measuring AL-adapted cells. As shown in Supplemental Figure 2, the fractions of photooxidizable (by a 22 ms saturating pulse), pre-oxidized in AL and non-photooxidizable P700 were determined by referring to the fully oxidized P700 signals in PSII-inhibited HA/DCMU samples (Buchert et al., 2020). Since the above-mentioned ECS slopes obtained during 2 ms AL are a function of the P700 oxidation rate in PSII-inhibited HA/DCMU samples, the obtained YI parameter in those samples served to calculate CEF (by multiplication with the P700 oxidation rate) as it a function of the concentration of reduced P700 in AL (Takahashi et al., 2013).

Chlorophyll fluorescence measurement

Cells were grown in liquid TP medium to ~1 × 10^6 cells$\cdot mL^{-1}$ with gentle shaking at 25°C under continuous light (50 µmol photons$\cdot m^{-2} \cdot s^{-1}$). The cells were harvested by centrifugation at 4000 rpm, suspended in fresh liquid TP medium at 5 µg Chl$\cdot mL^{-1}$, and placed in darkness for 30 min (growth light control samples). Photosynthesis driven by 450 nm LEDs was measured with a Maxi-Imaging PAM chlorophyll fluorometer (Heinz Walz, Germany). The effective photosynthetic active radiation

in the measuring chamber was determined with a Quantitherm PAR/Temp Sensor (Hansatech, England). Cell aliquots were also incubated shaking for 4 h under high light illumination (500 µmol photons·m^{-2}·s^{-1}). The maximal PSII quantum yield in dark-adapted samples and the PS II quantum yield during illumination Y(II) were determined as (Fm–Fo)/Fm and (Fm'–F)/Fm', respectively. Fo and Fm of dark-adapted samples are respective minimal (in the presence of detection light) and maximal fluorescence yields (due to closed PSII centers after saturating pulse). F and Fm' are the fluorescence yields in light-adapted cells obtained before and after a saturating pulse, respectively. The nonphotochemical quenching NPQ = (Fm–Fm')/Fm' was also determined, as well as estimation of the plastoquinone pool redox state using the (1–qL) parameter (Kramer et al., 2004). The latter required Fo' measurements (minimal fluorescence in illuminated samples) and qL was calculated as ((Fm'–F)×Fo')/((Fm'–Fo')×F). These parameters were either measured after 30 s during light curve experiments or at distinct time points when a 10 min continuous illumination at 95 µmol photons·m^{-2}·s^{-1} was applied.

Results

The PETC protein consists of one transmembrane helix and a lumenal hydrophilic domain in which Rieske iron sulfur cluster (ISC) is present, and both domains are connected through a flexible hinge. Based on the structural similarities with the Rieske subunit in bc_1 complex of respiratory chain, photosynthetic electron transfer between Rieske ISC and heme *f* in PetA involves reversible movements of the lumenal hydrophilic domain of PETC. The PETC amino acid sequence alignment shows that chloroplast targeting transit peptide of *A. thaliana* is 23 amino acids longer than that of *C. reinhardtii* while the mature protein sequence is highly conserved (Supplemental Figure 3). The four amino acids for ligation of two iron atoms and a flexible hinge region are conserved. Moreover, the mutated proline residue in Arabidopsis *pgr1* (Pro194) is conserved as Pro171 in *C. reinhardtii*. The location of this proline is close to Rieske ISC and is on the surface of hydrophilic domain (Figure 1B, C, and D), and its proximity to the Rieske ISC is conserved in the b_6f structures (Supplemental Figure 4).

Generation of *PETC-P171L* mutant in the green alga *Chlamydomonas reinhardtii*

The Arabidopsis *pgr1* mutant carrying single amino acid mutation in PETC (P194L) exhibits a hypersensitive photosynthetic control and downregulate the electron transfer flow under strong light illumination more strongly than wild type (Munekage et al., 2001). To characterize the corresponding PETC mutation in the green alga *C. reinhardtii*, we generated a *PETC-P171L* strain in which proline 171 is substituted by leucine. In our complementation-based screening approach, *petC-Δ1* was selected as a recipient strain since it has a frameshift upon TG base deletions within the 36th codon and does not accumulate *PETC* transcripts, thus showing no spontaneous reversion (de Vitry et al., 1999). Since the *petC-Δ1* exhibited a reduced accumulation of PSI protein, we backcrossed the *petC-Δ1* to wild type strain (cc-125) to assess whether the mutation of PETC gene affects the accumulation of PSI proteins. We obtained several tetrads and analyzed the accumulation of PsaA and PETC by immunoblotting (Figure 2). The $T_{15\text{-}3}$ progeny accumulates no PETC but PsaA normally and is referred to as the ΔPETC for the subsequent transformation since the two phenotypes were segregated. As described in Materials and Methods, we generated two types of vectors for transforming *PETC* gene; one consists

of genomic DNA fragment around PETC gene and the other contains PETC cDNA fused with *PSAD* promoter and UTRs. We delivered each transforming vector into the ΔPETC cells by electroporation and obtained numerous colonies after screening under photoautotrophic condition (on minimum solid medium in the light of 50 μmol photons·m^{-2}·s^{-1}). The resulting transformants recovered the accumulation of PETC to wild-type level, indicating that both vectors efficiently complemented the ΔPETC phenotype (Figure 3). Subsequently, we transformed ΔPETC with vectors containing the mutation PETC-P171L and obtained complemented strains expressing the mutated PETC. Immunoblot shows that the complemented PETC-P171L cells accumulated PETC as well as PetA at wild-type levels, suggesting that the mutation does not affect the stability of b_6f.

The *PETC-P171L* accumulates more oxidizable P700 and displays slower onset of electron transfer in anaerobic algae which relied on the lumen pH under these conditions.

Previous studies showed that high light treatment slows down ATP synthase activity in Chlamydomonas (Buchert et al., 2017), which eventually facilitates the induction of photosynthetic control. Since this type of H^+ conductivity regulation involves reactive oxygen species formation during photosynthetic electron transfer, which may differ between the strains, we chose a permissive light intensity for the following experiments (~160 μmol photons·m^{-2}·s^{-1} actinic red light) where this ATP synthase regulation is not expected. Instead, *pmf* partitioning was modulated on a metabolic level in light-adapted cells by lowering oxygen availability. A similar situation may occur in the natural habitat of Chlamydomonas which shares it with respiring microbes. Accordingly, the alga faces microoxic environments in which photosynthesis needs to be fine-tuned. Figure 4 shows a spectroscopic *in vivo* analysis of control and the *PETC-P171L* in oxic conditions and upon anaerobic treatment. Mitochondrial congestion in anoxic samples coincides with a redox poise shown to trigger CEF (Alric, 2014) and a *pmf* re-partitioning towards a more pronounced ΔpH (Finazzi and Rappaport, 1998).

Figures 4A and 4B display the redox state of P700, the primary electron donor of PSI (see Materials and Methods and Supplemental Figure 2 for representative kinetics). Under oxic conditions when PSII was active, the P700 redox states were indistinguishable between control and *PETC-P171L* (Figure

4A). About 20% of P700 were oxidized during actinic background light which is ascribed to similar donor side limitation (YND) in both strains. P700 was able to be further photooxidized by a short saturating light pulse, as shown by the yield of PSI (YI). A similar fraction (about 40%) of P700 was not oxidizable due to acceptor side limitation (YNA). On the contrary, YND was remarkably large when PSII was inhibited (HA+DCMU, Figure 4A) because electrons from PSII were suppressed. This coincided with YI of ~0.2 in control, i.e., 20% of P700 remained reduced in the light-adapted state in absence of PSII activity and were only oxidized by saturating pulses. This finding suggests that this 20% of P700 is reduced by electrons through CEF. YI in controls was roughly twice as large as in *PETC-P171L*, which translates in lower CEF rates in the mutant (indicated as 12 electrons$\cdot s^{-1} \cdot PSI^{-1}$ in parenthesis of Figure 4A).

Under anoxic conditions, control showed no significant difference in redox states of P700 (Figure 4B). However, the *PETC-P171L* established a larger YND and a lower YNA compared to control when PSII was active. In the absence of PSII activity, control and *P171L* showed similar P700 parameters. This finding shows that CEF rates in the steady state were unaffected in both strains (shown as electrons$\cdot s^{-1} \cdot PSI^{-1}$ in parenthesis of Figure 4B). Overall, we observed subtle differences on the level of light-adapted steady-state of P700. The differences were produced in the absence of PSII activity under oxic conditions and in the presence of PSII activity under anoxic conditions.

Next, we focused on the transition from dark to light, beginning with electrochromic shift measurements after 30-s darkness (Figure 4C). As mentioned above, a significant ΔpH is generated when algae are kept in the dark under anoxic conditions (Finazzi and Rappaport, 1998), which supposedly slows down the Qo-site activity in *PETC-P171L*. The electrochromic shift (ECS) of photosynthetic pigments allows to measure the membrane potential as the ECS signals linearly follow the electric *pmf* component (Junge and Witt, 1968; Witt, 1979). Figure 4C resolves the averaged *b*- and *c*-phases of the ECS kinetics produced by a sub-saturating laser flash (reviewed in Bailleul et al., 2010). The non-resolved *a*-phase with an amplitude of ~ 0.6 charge separations$\cdot PSI^{-1}$ relied on the charge separation activity of both photosystems. The *b*-phase, which is a ~10-ms ECS rise, involves charge separation activity via the b_6f and the *c*-phase depends on ATP synthase activity. The latter phase overlapped the *b*-phase since ATP synthase activity was driven by the *pmf* provided from

photosystem activity. Under oxic conditions, the fast *c*-phase prevented the appearance of a *b*-phase (Supplemental Figure 5). Therefore, the detection of an apparent *b*-phase requires a slow *c*-phase in anoxic algae (Velthuys, 1978). The ECS kinetics in anoxic *PETC-P171L* displayed a flat *b*-phase and comparably slow *c*-phase kinetics (Figure 4C), suggesting a compromised b_6f charge separation activity in *PETC-P171L*. To explore whether the b_6f performance during single turnover measurements affects the photosynthetic induction phase, we re-illuminated cells after a 30-s dark period. More specifically (see Materials and Methods), we measured electron transfer transients during the first 10-s of light in anoxic (Figure 4D) and oxic conditions (Figure 4E). The developing induction kinetics under anoxic conditions showed that the sum of LEF and CEF activities was transiently less efficient in *PETC-P171L*, producing the largest differences within the first 25 ms of light (cf. filled symbols and asterisk in Figure 4D). When PSII was inhibited (open symbols Figure 4D), no differences were observed between both strains. On the total electron transfer level, the induction kinetics were similar in both strains under oxic conditions (Figure 4E). The sum of LEF and CEF activities in the control strain was slightly higher at 4-s and 10-s of light (filled asterisks, Figure 4E). The kinetics were almost identical when PSII was inhibited, except for 100-ms of light where *PETC-P171L* produced slightly higher rates (open asterisk, Figure 4E).

To examine phenotype of anoxic *PETC-P171L* cells further, we repeated the electron transfer and P700 experiments in the presence and absence of nigericin (Figure 5). The H^+/K^+ ionophore exchanges the osmotic *pmf* component ΔpH for the electric one, ΔΨ. Thus, the drug was suitable to test the contribution of the previously reported ΔpH buildup (Finazzi and Rappaport, 1998), and its impact during the transition to sub-saturating light in dark-adapted anoxic *PETC-P171L*. Indeed, Figure 5A shows that nigericin action in the preceding 30-s of darkness abolished the *PETC-P171L* electron transfer bottleneck in the first ~50-ms of light. Moreover, the steady state rates were elevated in both strains when nigericin was present. In these cells, P700 redox states were changed upon nigericin addition (Figure 5B). In the absence of the drug, the control strain established a larger YNA and thus a smaller YI than *PETC-P171L*. The YND parameter was lowered to similar levels after adding nigericin. Upon nigericin addition, *PETC-P171L* cells established YNA and YI like control. Moreover, samples were indistinguishable in the absence of PSII activity (HA+DCMU, Figure 5B).

Taken together, these spectroscopic findings reveal that the P700 redox states under the actinic light illumination are differently distributed in *PETC-P171L* cells when oxygen levels were low. The different P700 redox state in *PETC-P171L* relied on upstream events on the level of the cytochrome b_6f and the ΔpH component of the *pmf* could be identified as being one of the limiting factors in oxygen-deprived algae. In most experiments at ~160 μmol photons·m^{-2}·s^{-1} actinic red light, *PETC-P171L* performed like control strains when cells were well aerated, suggesting that the acidification of the lumen pH in the permissive light was insufficient to trigger the cytochrome b_6f phenotype under these conditions. In the last two results sections, we will explore the *PETC-P171L* performance in the presence of oxygen at various light intensities.

The *PETC-P171L* mutant showed an impaired photoautotrophic growth rate under high light

We evaluated whether the *PETC-P171L* mutation has an impact on cellular growth over the course of days. The control and *PETC-P171L* cells grown in liquid medium were spotted on solid medium and the cell growth was observed (Figure 6A). The cells showed a similar photoheterotrophic growth under moderate light illumination on solid TAP medium. On the other hand, when cells were grown photoautotrophically on solid TP medium, *PETC-P171L* cells grew more slowly than control cells under illumination of 100 μmol photons·m^{-2}·s^{-1} and 600 μmol photons·m^{-2}·s^{-1}. Although the *PETC-P171L* cells were able to grow photoautotrophically, the relative growth rate of the mutant cells was apparently was slower in the stronger light (Figure 6A). We also analyzed the photoautotrophic growth of control and *PETC-P171L* strains in liquid medium under illumination of 200 μmol photons·m^{-2}·s^{-1}. We monitored the chlorophyll concentration of liquid culture as a measure of cell growth (Figure 6B). The doubling times of control and *PETC-P171L* were estimated to be 9.4 and 14 hours, respectively, indicating that *PETC-P171L* cells grow 1.5 times slowly under the high light condition.

The *PETC-P171L* shows an impaired NPQ induction under strong light illumination

The slower photoautotrophic growth of *PETC-P171L* cells may be ascribed to the lower activity of the mutated b_6f and/or to their stronger photosensitivity under strong light illumination. Then, we analyzed

the expression of LHCSR3 by immunoblotting since the protein is crucial for induction of algal NPQ. It was revealed that LHCSR3 was similarly induced after 4 h of strong light illumination in control and *PETC-P171L* cells (Figure 7A). Subsequently the induction of state transitions was also assessed by measuring fluorescence emission spectra at 77K. It was shown that control and the *PETC-P171L* cells exhibited higher intensity of PSII core fluorescence emission (peaking at 688 nm) in state 1 while the PSI core fluorescence emission (peaking at 716 nm) was higher in state 2, indicating both state 1 and state 2 were fully induced (Figure 7B). Thus, the PETC-P171L mutation showed normal expression of LHCSR3 and induction of state transitions.

Next, we measured light-dependent steady state chlorophyll fluorescence parameters under high light conditions and, like in Figure 7A, the analyzed *PETC-P171L* cells showed control-like LHCSR3 accumulation upon high light treatment (Figure 8A). The latter observation ensured that NPQ could be measured *per se*. As expected, PAM fluorimetry light curve experiments revealed low NPQ in both strains which were not exposed to 4 h high light (cf. filled symbols in Figure 8B). Interestingly, only control cells showed increased NPQ when pre-treated in high light (cf. open symbols in Figure 8B). The PSII quantum yield Y(II) was very similar between the strains at irradiances below 30 µmol photons$\cdot$m$^{-2}\cdot$s^{-1} of actinic blue light, except for the Fv/Fm in high light treated cells which was lower in *PETC-P171L* (cf. Y(II) at lowest irradiance, inset in Figure 8C). At higher irradiances, Y(II) in controls was above that in *PETC-P171L* irrespective of high light pre-treatment (Figure 8C). The NPQ induction over a 10 min light period indicated that a lower capacity in *PETC-P171L*, and that high light exposure stimulated NPQ only in the control strain (Figure 8D). After the 10 min light, NPQ collapsed rapidly within the first 30 s of darkness which was followed by a transient NPQ increase. The Y(II) was lowest in the mutant during 10 min of illumination, but the values recovered similarly in all strains during subsequent darkness (Figure 8E). The related (1-qL), indicative for the PQ pool reduction state, was highest in illuminated *PETC-P171L* and the NPQ-displaying control strains maintained a more oxidized PQ pool during 10 min of light (Figure 8F). Taken together, the chlorophyll fluorescence parameters in *PETC-P171L* suggested a limitation of photosynthesis at elevated irradiances on the level of cytochrome b_6f complex.

Discussion

In the current work we successfully generated a *PETC-P171L* strain in *C. reinhardtii,* harboring a genetic site-directed alteration corresponding to the mutation in *pgr1* of *A. thaliana* (Shikanai et al., 1999; Munekage et al., 2001; Jahns et al., 2002; Okegawa et al., 2005). In *C. reinhardtii*, this mutation did not affect b_6f accumulation but diminished the electron transfer rate due to lumenal acidification. In Arabidposis, the *pgr1* mutant showed reduced NPQ owing to cessation of total electron transfer at the level of b_6f at elevated light intensities above ~200 µmol photons·m^{-2}·s^{-1} (Munekage et al., 2001). It was further found that the pH-dependent inactivation of electron transfer via the b_6f was shifted by about 1 pH unit towards more alkaline pH values using *pgr1* thylakoids from Arabidopsis (Jahns et al., 2002). Our data indicated similar effects that *PETC-P171L* is sensitive to high light due to an inefficient photosynthesis. The algal mutant was capable of state transitions but grew slower, and anoxic treatment revealed that the ΔpH-dependent slow-down of electron transfer through the PETC-P171L b_6f complex was already induced at lower light intensities.

The PETC-P171L mutation slows down the electron transfer through b_6f in lumenal pH acidification.

The previous studies observed strong NPQ reduction in *pgr1* after high light illumination, linked to suppression of electron transfer in the mutant plants (Munekage et al., 2001; Okegawa et al., 2005; Yamamoto and Shikanai, 2019). Our investigation of factors triggering photosynthetic control in algae revealed similarities to vascular plants, i.e., the bottleneck of electron transfer in *PETC-P171L* was detected in high light conditions (Figure 8). We ruled out that state transitions were affected by the Qo-site mutation (Figure 7) and also evaluated the photosynthetic machinery of *PETC-P171L* during permissive actinic illumination (Figures 4 and 5). The light intensity was kept low to avoid a potential source of variability by a downregulation of ATP synthase as a side effect of photosynthesis in high light (Buchert et al. 2017). Here, we identified a significant b_6f defect in *PETC-P171L* under anoxia which had an impact on faster electron flow cessation during photosynthetic induction and facilitated P700 oxidation in the light. The addition of nigericin, exchanging ΔpH for ΔΨ, abolished the impact of the mutation. Anaerobiosis increases the ΔpH contribution to the *pmf* in darkness, which depends

on functional ATP synthase (Finazzi and Rappaport, 1998; Rappaport et al., 1999). Oxygen deprivation caused a charge separation deficiency of the b_6f in *PETC-P171L*, which is a consequence of delayed mutant Qo-site turnover. In fact, a cooperativity of high- and low-potential chain reactions has been documented in previous Rieske iron sulfur protein (ISP) mutants of the cytochrome bc_1 complex from yeast (Snyder et al., 2000). Still, this coupling mechanism operating between Qo- and Qi-site remains elusive. The authors mutated homologous Rieske ISP residues at position 157 and 159 (orange-colored rectangle in Supplemental Figure 3), not too far from proline 171 of *C. reinhardtii* PETC, which eventually result in a more reducing E_m and a slowdown of *b*-heme reduction (Snyder et al., 2000). Thus, similar effects could be anticipated in *PETC-P171L* provided that the mutation lowers the Rieske ISP E_m b_6f as originally proposed (Munekage et al., 2001; Jahns et al., 2002). However, the Rieske ISP E_m potential has not been determined in *pgr1*. Previous data indicated that the E_m potential of reconstituted recombinant *C. reinhardtii* Rieske ISP is pH-dependent with a pK_{ox} of 6.2 and a pK_{red} of 8.2 (Soriano et al., 2002). The ISP E_m potential changes in the pH-dependent region with -40mV/pH. Thus, lowering the Rieske ISP E_m via the PETC-P171L mutation could impact pK_{ox} and pK_{red} and might alter inter b_6f electron transfer as shown in yeast (Snyder et al., 2000). In an alternative scenario, the PETC-P171L mutation might alter binding of PQH_2 to the Q_o-site and consecutively change the pH-dependent redox properties and oxidation of PQH_2. The Rieske ISC is found in the hydrophilic domain of PETC (Figure 1B) and, based on structural similarities with bc_1 complex (Darrouzet, Valkova-Valchanova, Moser, Dutton, & Daldal, 2000), it is supposed to be a flexible hydrophilic domain to realize electron transfer between redox centers Rieske ISC and heme *f*. Additionally, proline 171 mutated in this study is the second proline of the "Proline-X-Proline" motif, which is a common structure at the beginning of turn structure (MacArthur & Thornton, 1991). This motif is exclusively found in PETC protein and conserved among Rieske ISP (Supplemental Figure 3). Accordingly, this motif forms a typical hairpin structure and the substitution of the second proline to leucine may disturb conformation of PETC hydrophilic domain structure, causing the functional impact in the redox chemistry of b_6f.

Our findings revealed that the generated ΔpH in anaerobic Chlamydomonas during 30-s of darkness was sufficient to trigger severe photosynthetic control in *PETC-P171L*, preventing efficient *b*-hemes

reduction. Moreover, the nigericin data also revealed an important contribution of the ΔpH in anaerobic cells. Accordingly, b_6f regulation is important for PSI photoprotection in a reducing cellular environment such as anaerobiosis. The differential regulation of pH dependent inactivation of electron transfer via the b_6f in oxic and anoxic conditions in *PETC-P171L* is surprising. This might suggest that depending on oxygen availability (or metabolic congestion), the regulation of photosynthetic control is distinct in *C. reinhardtii*. However, revealing a low-light *pgr1* phenotype may also occur in plants when metabolism becomes restricted, e.g. under drought stress conditions where a downregulated ATP synthase activity favors large ΔpH amplitudes (Kohzuma et al., 2009). How can this be rationalized? Three non-exclusive scenarios may occur: First, metabolic control of ATP synthase downregulates H^+ conductivity which theoretically facilitates a light-dependent ΔpH build up in anaerobic conditions. Second, sustaining a ΔpH in an ATP synthase-dependent manner is favored in anoxic algae even in darkness (Finazzi and Rappaport, 1998; Rappaport et al., 1999). Third, the regulation of b_6f electron transfer via the Q-cycle is distinct under oxic and anoxic conditions (Buchert et al., 2020). Under anoxic conditions stromal electron intake into b_6f changes the Q-cycle from a canonical cycle during LEF to an alternative cycle during CEF, which would facilitate more efficient proton translocating into the lumen as compared with the canonical Q-cycle (Buchert et al., 2020). In line, photosynthetic control would be faster activated under anoxia and revealed the *PETC-P171L* phenotype even in low-light conditions.

Taken together, *PETC-P171L* may be a useful tool for future investigations under various metabolic and environmental conditions to uncover details of the cooperative mechanism between Qo- and Qi-site. Moreover, *PETC-P171L* may help to elucidate the interplay of various *pmf*-shaping ion channels/antiporters involved to fine-tune *pmf* partitioning in algae in response to metabolic constraints.

PETC-P171L mutation retards photoautotrophic cell growth.

The growth phenotype of *pgr1* plants under different light intensities has not been addressed in literature (Shikanai et al., 1999; Munekage et al., 2001; Yamamoto and Shikanai, 2019). We found

that *PETC-P171L* grew less efficiently under photoautotrophic condition at growth rates 1.5 times slower in the logarithmic phase than control (Figure 6 and Supplemental Figure 6). Despite similar amounts of LHCSR3 in the control and *PETC-P171L* cells, NPQ could not be fully established in *PETC-P171L* and PSII performance was low due to a more reduced PQ pool in the mutant (Figures 7 and 8). This analysis shows the *PETC-P171L* mutation impacts cellular growth and underlines the importance of a balanced photosynthetic control in wild type cells (control strain), avoiding premature cessation of photochemistry as a function of light intensity.

Taken together, *PETC-P171L* exhibits a reduced photosynthetic electron transfer rate because of its hypersensitive photosynthetic control mechanism. The light intensity threshold to trigger the hypersensitive effect in the mutant b_6f can be modulated by the metabolic state of the cell. The molecular machinery to realize energy quenching and balancing of light harvesting is established as in wild type b_6f strains. These results are consistent with Arabidopsis studies, indicating that the effect of the proline substitution in PETC on electron transfer is *per se* conserved between the two organisms.

Acknowledgement

The *petC-Δ1*strain and pACR4.5 plasmid were kindly gifted by Catherine de Vitry. The cDNA library of *C. reinhardtii* and the pSL18 plasmid expression vector were provided by Michel Goldschmidt-Clermont. The antibodies against PsaA and PetA/PETC were kindly gifted by Kevin Redding and Olivier Vallon, respectively.

1 **Figures**

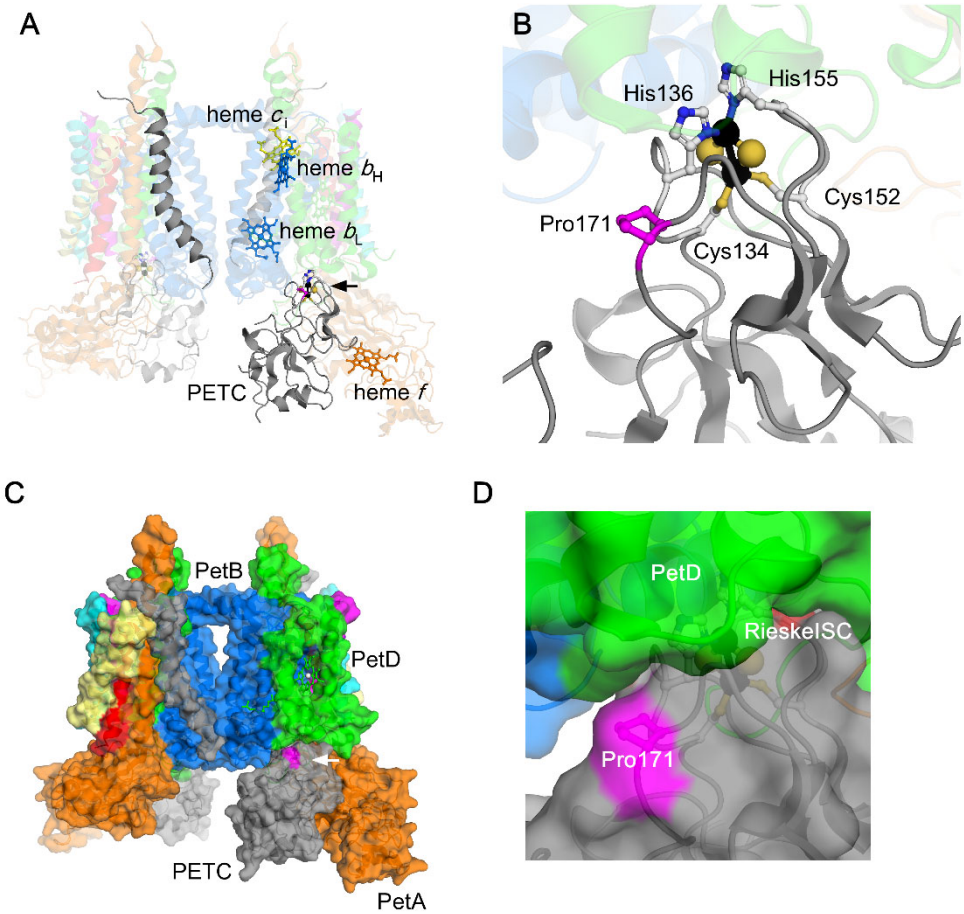

2 **Figure 1**

3 **The position of Rieske ISC and PETC-Pro171 in the Chlamydomonas b_6f complex**

4 Structures of the dimeric b_6f from the *C. reinhardtii* (PDB; 1Q90). The flexible hinge of PETC is not
5 modeled. The Rieske ISCs are shown in space filling representation and of which ligand amino acids
6 (Cys134, His136, Cys152, and His155 of PETC) and Pro171 of PETC (colored in magenta) and four
7 hemes (heme c_i is yellow, heme b_H and heme b_L are blue, and heme f is orange) are shown in ball-stick
8 model. The PetA (orange), PetB (blue), PETC (gray), PetB (green), PetG (magenta), PetL (yellow),
9 PETM (cyan), and PETN (red) subunits are shown. **(A)** and **(C)**. Overall structure with the lumenal
10 side at bottom and the stromal side at the top. The position of one of the Rieske ISC is indicated with
11 arrow. **(B)** and **(D)**. The enlarged view around the Rieske iron sulfur cluster. **(C)** and **(D)**. Protein
12 surface is modeled. The subunits and cofactors except for PETC subunit are transparent in panel A and
13 B.

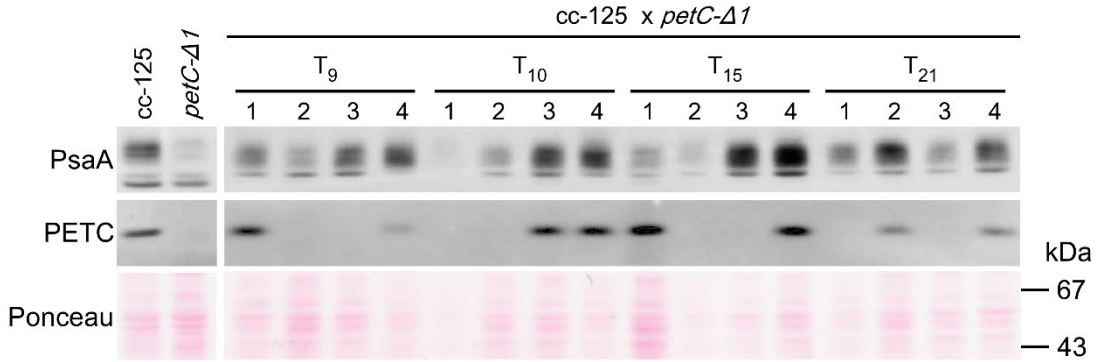

1 **Figure 2**

2 **Isolation of PSI suppression free PETC deleted strain**

3 The *petC-Δ1* was backcrossed with cc-125 and the resultant progenies were analyzed by
4 immunoblotting using the antibodies against PsaA or PETC. Whole cellular proteins (0.5 μg Chl per
5 lane) were denatured, separated by SDS-PAGE, and analyzed by immunoblot. The polypeptides
6 transferred on nitrocellulose membrane were stained with Ponceau (the migration positions of protein
7 standard are shown). The proteins of progenies (1 to 4) from four independent perfect tetrads (T_9, T_{10},
8 T_{15}, and T_{21}) and their parent strains (cc-125 and *petC-Δ1*) are loaded.

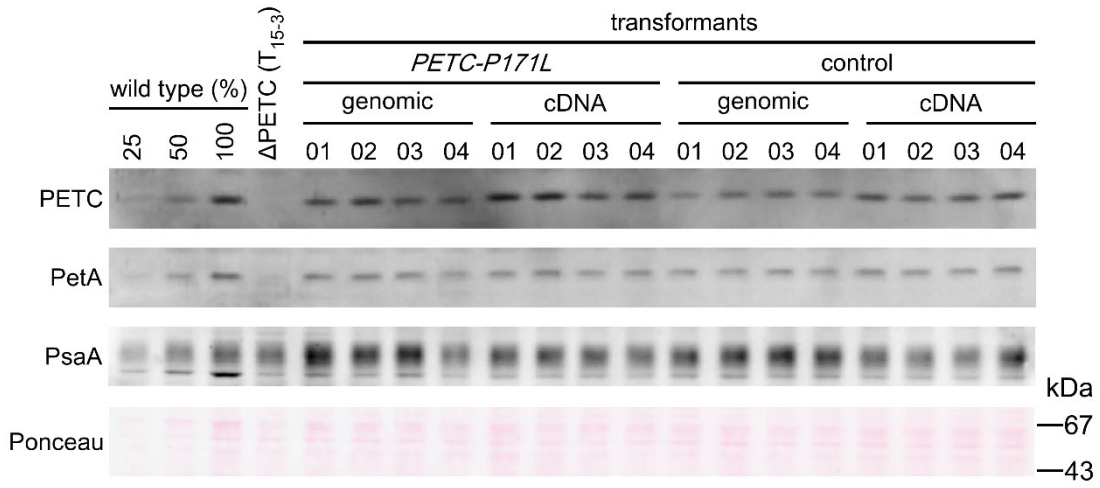

1 **Figure 3**

2 **Generation of *PETC-P171L* mutant**

3 The accumulation of PSI (PsaA) and b_6f (PETC and PetA) proteins was analyzed by immunoblotting.
4 The cells were grown in TAP liquid medium in the light of 50 μmol photons·m^{-2}·s^{-1}. The Pro171Leu
5 of PETC (*PETC-P171L*) and wild type sequence of PETC (control), the PETC gene expressing with
6 own promoter and UTRs (genomic) or the spliced PETC gene expressing with PSAD promoter UTRs
7 (cDNA). Four independent clones from each transformant, a dilution series for the wild type (wild
8 type (%)), and ΔPETC ($T_{15\text{-}3}$ in Figure 2) were also analyzed.

1 **Figure 4**

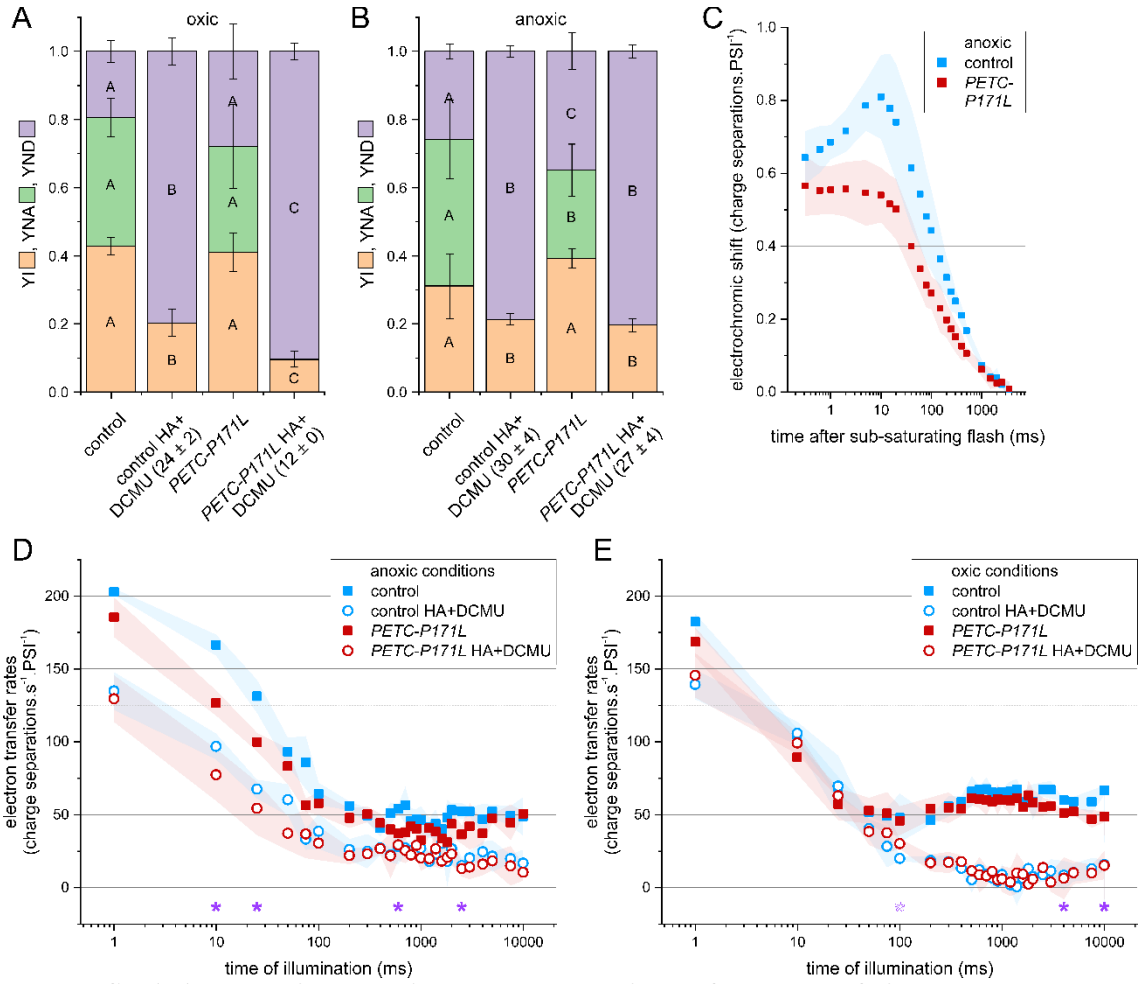

2 **The *PETC-P171L* mutation restricts photosynthetic performance of light- and dark-adapted**
3 **cells predominantly in anaerobic conditions.**

4 P700 redox states were measured in **(A)** oxic and **(B)** anoxic light-adapted cells. The fractional yields
5 of P700 in the photo-oxidizable state (YI), the non-oxidizable form due to acceptor side limitation
6 (YNA), and the pre-oxidized P700 due to donor side limitation (YND) are shown (parameter-specific
7 one-way ANOVA, $n = 3$, $P < 0.05$). The oxic controls in absence of PSII activity (HA+DCMU)
8 retained a higher YI due to enhanced steady state CEF (expressed charge separations·s^{-1}·PSI^{-1} ± SD).
9 In anoxic conditions, *PETC-P171L* failed to establish the YNA due to larger YND. **(C)** The
10 electrochromic shift ~10-ms rising phase, associated with charge separation activity upon a single b_6f
11 turnover, was less pronounced in anoxic light-adapted *PETC-P171L*. Sub-saturating flashes were fired
12 on light-adapted cells after a 30-s dark period (averaged kinetics ± SD, $n = 3$). **(D)** After a 30-s dark
13 period, electron transfer rates over a 10-s photosynthetic induction phase were measured in anoxic

light-adapted cells. Total electron transfer in *PETC-P171L* was significantly less efficient at discrete time points, especially in the initial ~25-ms (filled asterisk, Student's t-test $P < 0.05$). A significant difference during induction required PSII activity. **(E)** The induction phase was indistinguishable in oxic conditions. Total electron transfer rates in the controls were enhanced at a later stage of illumination (filled asterisks), and *PETC-P171L* showed transiently higher rates at 100-ms in absence of PSII activity (open asterisk).

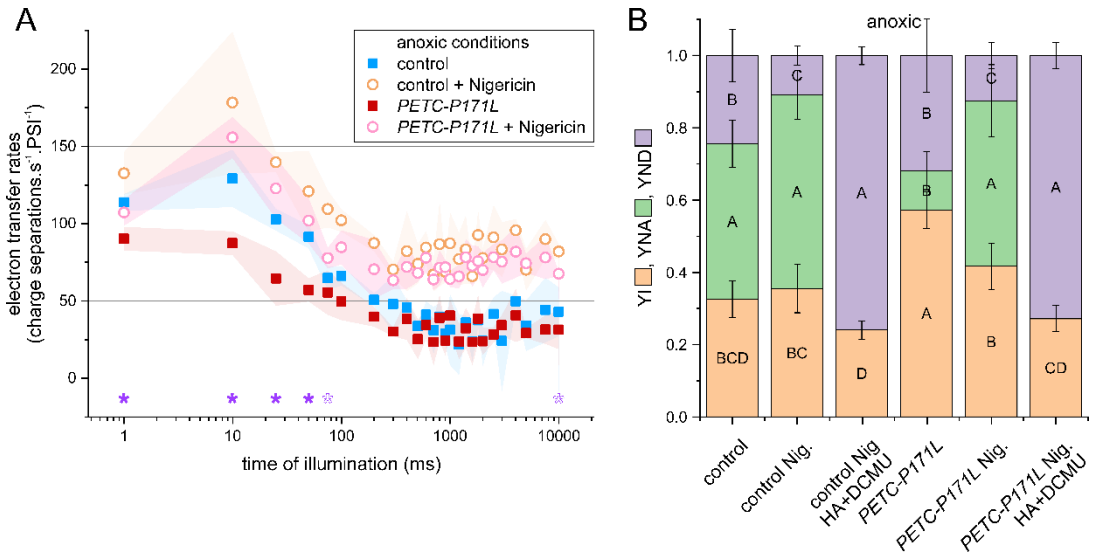

1 **Figure 5**

2 **The electron transfer restrictions in *PETC-P171L* cells under anaerobic conditions is overcome**
3 **by diminishing the ΔpH via nigericin.**

4 **(A)** After a 30-s dark period, electron transfer rates over a 10-s photosynthetic induction phase were
5 measured in anoxic light-adapted cells (averaged kinetics ± SD, n = 3). Total electron transfer in
6 *PETC-P171L* was significantly less efficient within the first ~50-ms (filled asterisk, Student's t-test P
7 < 0.05). The different induction kinetics between the strains relied on the ΔpH and became similar
8 after addition of the H^+/K^+ ionophore nigericin (Nig., 10 µM), although the control showed higher
9 rates at discrete sampling intervals (open asterisk). In both strains the steady state rates were higher
10 when Nig. was present. **(B)** On the level of co-dependent PSI parameters, the fractional yields of P700
11 in the photo-oxidizable state (YI), the non-oxidizable form due to acceptor side limitation (YNA), and
12 the pre-oxidized P700 due to donor side limitation (YND) are shown (parameter-specific one-way
13 ANOVA, n = 3, P < 0.05). The YI was larger in *PETC-P171L* owing to a diminished YNA. YND was
14 lowered to similar levels after adding Nig. and diminishing ΔpH-dependent photosynthetic control.
15 Moreover, further PSII inhibition (HA+DCMU) produced similar P700 yields.

16

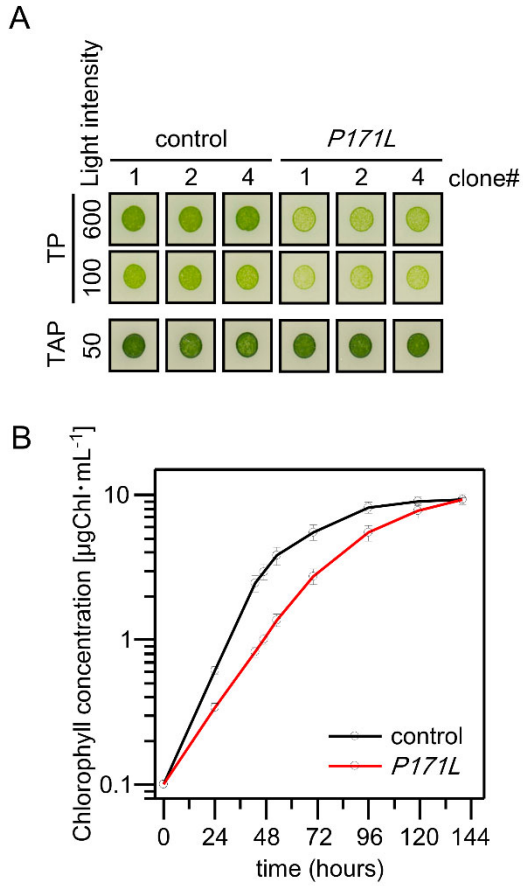

1 **Figure 6**

2 **The photoautotrophic growth rate is slowed down at low cell density in *PETC-P171L*.**

3 **(A)** Cells were grown photoheterotrophically on solid TAP medium (50 µmol photons·m^{-2}·s^{-1}) or

4 photoautotrophically on solid TP medium (100 or 600 µmol photons·m^{-2}·s^{-1}). Three independent

5 clones of the control and *PETC-P171L* strain (*P171L*) were analyzed. **(B)** Photoautotrophic cell

6 growth is monitored by measuring Chlorophyll concentration of the TP liquid culture medium grown

7 under continuous light (200 µmol photons·m^{-2}·s^{-1}). Black line represents control and red line

8 represents *PETC-P171L (P171L)*. Three biological replicates were averaged (± standard errors).

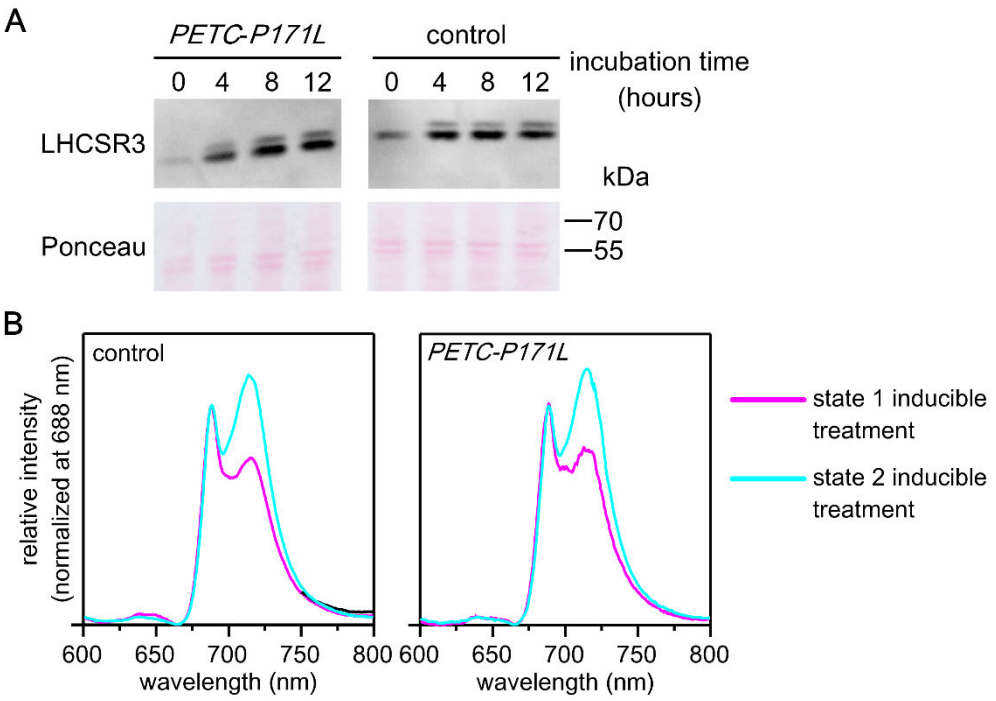

Figure 7

The *PETC-P171L* mutation does neither affect LHCSR3 expression induction and/or stability, nor induction of state-transitions.

(A) The cells grown in TP medium were shifted from low light (15 µmol photons·m^{-2}·s^{-1}) to stronger light (200 µmol photons·m^{-2}·s^{-1}) and immune-chase experiment with the antibody against LHCSR3 protein was performed for cellular proteins. Cells were harvested before shifting to higher light (0), after 4, 8, 12, and 24 hours shifting to high light. Ponceau staining panel served as loading control. **(B)** The TP-grown Chlamydomonas cells acclimated under high light (300 µmol photons·m^{-2}·s^{-1}) were resuspended with TP at 2 µg Chlorophyll·mL^{-1} and incubated in state 1 or state 2 inducible condition. In the case of state 1 inducible treatment, cells were incubated under 200 µmol photons·m^{-2}·s^{-1} in the presence of DCMU for 10 minutes. In the case of state 2 inducible treatment, cells were incubated in the darkness for 10 minutes in the presence of 100 mM glucose and 50 U·mL^{-1} glucose oxidase. Samples were excited with 430 nm and the emitted fluorescence were recorded from 600 to 800 nm in liquid nitrogen. The fluorescence spectra were normalized at 688 nm.

1 **Figure 8**

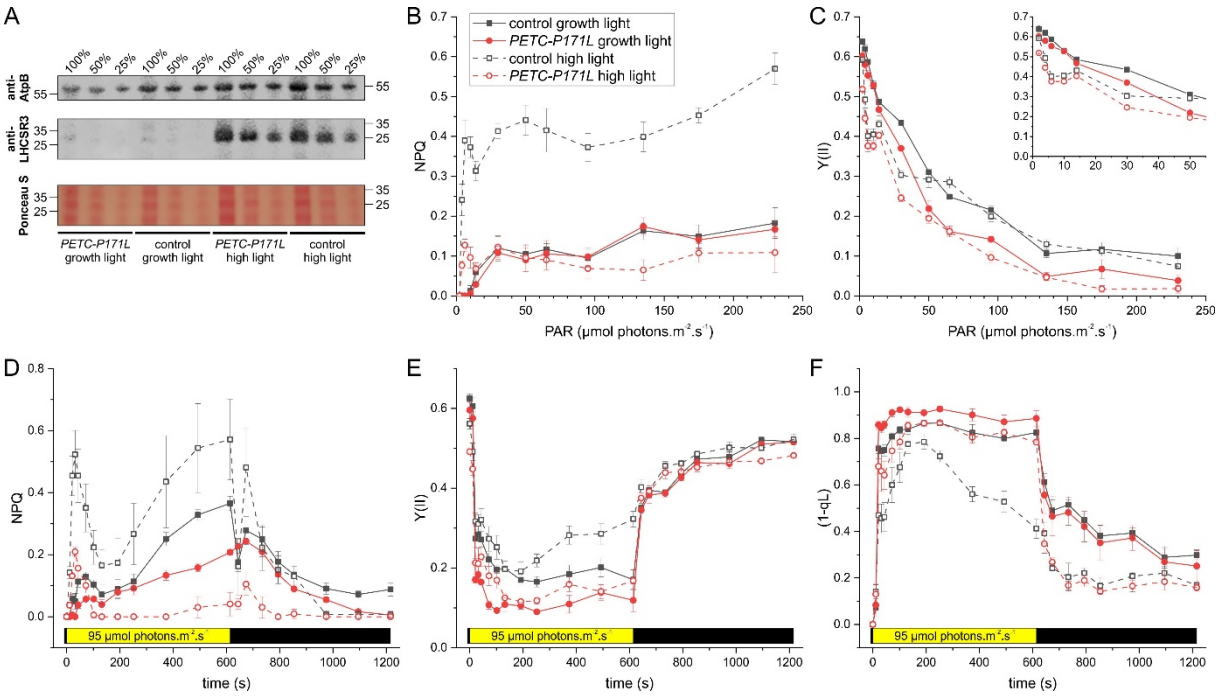

2

3 **The chlorophyll fluorescence parameters reveal a limited photosynthetic capacity in *PETC-***
4 ***P171L*.**

5 **(A)** Immunodetection of LHCSR3 protein was obtained from growth light samples (50 µmol
6 photons·m^{-2}·s^{-1}) and after 4 h high light treatment (500 µmol photons·m^{-2}·s^{-1}). Based on chlorophyll
7 loading (100% = 3 µg) and the AtpB reference, LHCSR3 accumulation and induction was comparable
8 in the control and *PETC-P171L* cells. A representative Western Blot is shown and the chlorophyll
9 fluorescence parameters in panels B to F are means three biological replicates (± standard deviations).
10 **(B)** The control strains showed more NPQ during light curve experiments which was further increased
11 upon high light treatment, unlike in *PETC-P171L*. **(C)** The PSII quantum yield, Y(II), was comparable
12 in growth light samples up to 30 µmol photons·m^{-2}·s^{-1} of actinic light (inset), and Y(II) remained
13 higher in the control strains when light was further increased. The strain-specific Y(II) developments
14 showed a similar trend in high light samples. **(D)** The NPQ induction over 10 min of light was more
15 efficient in control strains irrespectively of high light pre-treatment, although it enhanced NPQ
16 capacity. **(E)** The corresponding Y(II) was also lower in *PETC-P171L* during the light period. The
17 Y(II) in high light treated mutants increased rapidly upon transition to darkness and **(F)** the increased

(1-qL) in those samples suggested a strongly reduced plastoquinone pool during the preceding illumination.

References

Alric J (2014) Redox and ATP control of photosynthetic cyclic electron flow in Chlamydomonas reinhardtii: (II) involvement of the PGR5-PGRL1 pathway under anaerobic conditions. Biochim Biophys Acta 1837: 825-834

Bailleul B, Cardol P, Breyton C, Finazzi G (2010) Electrochromism: a useful probe to study algal photosynthesis. Photosynth Res 106: 179-189

Bonente G, Ballottari M, Truong TB, Morosinotto T, Ahn TK, Fleming GR, Niyogi KK, Bassi R (2011) Analysis of LhcSR3, a protein essential for feedback de-excitation in the green alga Chlamydomonas reinhardtii. PLoS Biol 9: e1000577

Buchert F, Bailleul B, Hisabori T (2017) A gamma-subunit point mutation in Chlamydomonas reinhardtii chloroplast F1Fo-ATP synthase confers tolerance to reactive oxygen species. Biochim Biophys Acta Bioenerg 1858: 966-974

Buchert F, Hamon M, Gabelein P, Scholz M, Hippler M, Wollman FA (2018) The labile interactions of cyclic electron flow effector proteins. J Biol Chem 293: 17559-17573

Buchert F, Mosebach L, Gabelein P, Hippler M (2020) PGR5 is required for efficient Q cycle in the cytochrome b6f complex during cyclic electron flow. Biochem J 477: 1631-1650

de Vitry C, Finazzi G, Baymann F, Kallas T (1999) Analysis of the nucleus-encoded and chloroplast-targeted rieske protein by classic and site-directed mutagenesis of Chlamydomonas. Plant Cell 11: 2031-2044

Delepelaire P, Wollman FA (1985) Correlations between fluorescence and phosphorylation changes in thylakoid membranes of Chlamydomonas reinhardtii in vivo: A kinetic analysis. Biochimica et Biophysica Acta (BBA) - Bioenergetics 809: 277-283

Depège N, Bellafiore S, Rochaix JD (2003) Role of chloroplast protein kinase Stt7 in LHCII phosphorylation and state transition in Chlamydomonas. Science 299: 1572-1575

Finazzi G, Rappaport F (1998) In vivo characterization of the electrochemical proton gradient generated in darkness in green algae and its kinetic effects on cytochrome b6f turnover. Biochemistry 37: 9999-10005

Harris EH (1988) The Chlamydomonas Sourcebook. Academic Press, San Diego

Jahns P, Graf M, Munekage Y, Shikanai T (2002) Single point mutation in the Rieske iron-sulfur subunit of cytochrome b6/f leads to an altered pH dependence of plastoquinol oxidation in Arabidopsis. FEBS Lett 519: 99-102

Jokel M, Johnson X, Peltier G, Aro EM, Allahverdiyeva Y (2018) Hunting the main player enabling Chlamydomonas reinhardtii growth under fluctuating light. Plant J 94: 822-835

Joliot P, Joliot A (2002) Cyclic electron transfer in plant leaf. Proc Natl Acad Sci U S A 99: 10209-10214

Junge W, Witt HT (1968) On the ion transport system of photosynthesis--investigations on a molecular level. Z Naturforsch B 23: 244-254

Kanazawa A, Kramer DM (2002) In vivo modulation of nonphotochemical exciton quenching (NPQ) by regulation of the chloroplast ATP synthase. Proc Natl Acad Sci U S A 99: 12789-12794

Klughammer C, Schreiber U (1994) An improved method, using saturating light pulses, for the determination of photosystem I quantum yield via $P700^{+}$-absorbance changes at 830 nm. Planta 192: 261-268

Kohzuma K, Cruz JA, Akashi K, Hoshiyasu S, Munekage YN, Yokota A, Kramer DM (2009) The long-term responses of the photosynthetic proton circuit to drought. Plant Cell and Environment 32: 209-219

Kramer DM, Johnson G, Kiirats O, Edwards GE (2004) New fluorescence parameters for the determination of Q_A redox state and excitation energy fluxes. Photosynth Res 79: 209

Kurisu G, Zhang H, Smith JL, Cramer WA (2003) Structure of the cytochrome b6f complex of oxygenic photosynthesis: tuning the cavity. Science 302: 1009-1014

Munekage Y, Takeda S, Endo T, Jahns P, Hashimoto T, Shikanai T (2001) Cytochrome b(6)f mutation specifically affects thermal dissipation of absorbed light energy in Arabidopsis. Plant J 28: 351-359

Nawrocki WJ, Bailleul B, Cardol P, Rappaport F, Wollman FA, Joliot P (2019) Maximal cyclic electron flow rate is independent of PGRL1 in Chlamydomonas. Biochim Biophys Acta Bioenerg 1860: 425-432

Nishio JN, Whitmarsh J (1993) Dissipation of the Proton Electrochemical Potential in Intact Chloroplasts (II. The pH Gradient Monitored by Cytochrome f Reduction Kinetics). Plant Physiol 101: 89-96

Okegawa Y, Tsuyama M, Kobayashi Y, Shikanai T (2005) The pgr1 mutation in the Rieske subunit of the cytochrome b6f complex does not affect PGR5-dependent cyclic electron transport around photosystem I. J Biol Chem 280: 28332-28336

Peers G, Truong TB, Ostendorf E, Busch A, Elrad D, Grossman AR, Hippler M, Niyogi KK (2009) An ancient light-harvesting protein is critical for the regulation of algal photosynthesis. Nature 462: 518-521

Pfefferkorn B, Meyer HE (1986) N-terminal amino acid sequence of the Rieske iron-sulfur protein from the cytochrome b6/f-complex of spinach thylakoids. FEBS Letters 206: 233-237

Pierre Y, Breyton C, Kramer D, Popot JL (1995) Purification and characterization of the cytochrome b6 f complex from Chlamydomonas reinhardtii. J Biol Chem 270: 29342-29349

Rappaport F, Finazzi G, Pierre Y, Bennoun P (1999) A new electrochemical gradient generator in thylakoid membranes of green algae. Biochemistry 38: 2040-2047

Rumberg B, Siggel U (1969) pH changes in the inner phase of the thylakoids during photosynthesis. Naturwissenschaften 56: 130-132

Shikanai T, Munekage Y, Shimizu K, Endo T, Hashimoto T (1999) Identification and characterization of Arabidopsis mutants with reduced quenching of chlorophyll fluorescence. Plant Cell Physiol 40: 1134-1142

Snyder CH, Gutierrez-Cirlos EB, Trumpower BL (2000) Evidence for a concerted mechanism of ubiquinol oxidation by the cytochrome bc1 complex. J Biol Chem 275: 13535-13541

Soriano GM, Guo LW, De Vitry C, Kallas T, Cramer WA (2002) Electron transfer from the Rieske iron-sulfur protein (ISP) to cytochrome f in vitro. Is a guided trajectory of the ISP necessary for competent docking? J Biol Chem 277: 41865-41871

Stroebel D, Choquet Y, Popot JL, Picot D (2003) An atypical haem in the cytochrome b_6f complex. Nature 426: 413-418

Sueoka N (1960) MITOTIC REPLICATION OF DEOXYRIBONUCLEIC ACID IN CHLAMYDOMONAS REINHARDI. Proc Natl Acad Sci U S A 46: 83-91

Takahashi H, Clowez S, Wollman FA, Vallon O, Rappaport F (2013) Cyclic electron flow is redox-controlled but independent of state transition. Nat Commun 4: 1954

Takahashi H, Schmollinger S, Lee JH, Schroda M, Rappaport F, Wollman FA, Vallon O (2016) PETO Interacts with Other Effectors of Cyclic Electron Flow in Chlamydomonas. Mol Plant 9: 558-568

Tikhonov AN, Khomutov GB, Ruuge EK, Blumenfeld LA (1981) Electron transport control in chloroplasts. Effects of photosynthetic control monitored by the intrathylakoid pH. Biochimica et Biophysica Acta (BBA) - Bioenergetics 637: 321-333

Velthuys BR (1978) A third site of porton translocation in green plant photosynthetic electron transport. Proc Natl Acad Sci U S A 75: 6031-6034

Witt HT (1979) Energy conversion in the functional membrane of photosynthesis. Analysis by light pulse and electric pulse methods. The central role of the electric field. Biochim Biophys Acta 505: 355-427

Yamamoto H, Shikanai T (2019) PGR5-Dependent Cyclic Electron Flow Protects Photosystem I under Fluctuating Light at Donor and Acceptor Sides. Plant Physiol 179: 588-600

Yamano T, Iguchi H, Fukuzawa H (2013) Rapid transformation of Chlamydomonas reinhardtii without cell-wall removal. J Biosci Bioeng 115: 691-694

Yan J, Cramer WA (2003) Functional insensitivity of the cytochrome b6f complex to structure changes in the hinge region of the Rieske iron-sulfur protein. J Biol Chem 278: 20925-20933